COBEM 2021 26th International Congress of Mechanical Engineering
November 22-26, 2021, Virtual Congress, Brazil

COB-2021-1784
UNCERTAINTIES ASSESSMENT ON THE INFRARED THERMOGRAPHY CALIBRATION TECHNIQUES

Victor E. C. Baptistella
Gherhardt Ribatski
Heat Transfer Research Group, São Carlos School of Engineering, University of São Paulo, São Carlos, SP, Brazil
victor.baptistella@usp.br
ribatski@sc.usp.br

Abstract. *Infrared thermography is a powerful technique to measure surface temperatures and evaluate heat transfer coefficients during dynamic thermal processes such as pool and flow boiling, jet impingement and drop evaporation. To do that, the test section must allow optical access to the surface under study in the IR spectrum, which is obtained through the following methods: (i) using a metal foil or channel covered with a high emissivity paint on the outside surface; (ii) using a thin conducting film deposited on an IR transparent or semi-transparent substrate. The film heater is in direct contact with the fluid and the substrate is interposed between the heater and the camera. The first configuration has the advantage of being simple and allowing the use of a polynomial curve fit to map the IR signal into surface temperatures. However, the heat diffusion through the channel wall damps the temperature variations of the inner wall, limiting the observed time scales, and in the case of the foil, it is not representative of real surfaces due to its low heat capacity. The second configuration, although more complex, allows the evaluation of the inner surface temperature distribution without wall damping effects, however, its application needs either a negligible effect of the substrate on the signal reaching the camera sensor or a calibration procedure to compensate the substrate effects. This work aims at the comparison of data reduction and calibration techniques developed for temperature measurements in an Indium Tin Oxide (ITO)-sapphire heater using an IR camera. Although sapphire has non-negligible IR absorption, it is commonly used, because of its mechanical properties in comparison to materials such as calcium fluoride, which is fragile but has negligible IR absorption. The errors provided by the polynomial curve fit and different calibration models are parametrically compared. These models separate the irradiated energy reaching the camera into heater, substrate, and ambient energy, by solving a radiation-conduction coupled system of equations and can be based on averaged optical properties and wavelength-dependent properties. It is found that when the substrate temperature field is non-uniform, the calibration curve does not provide accurate estimations of the heated surface temperature and the spectral dependency of the heater optical properties must be precisely known, otherwise the errors are high even using complex calibration models. Additionally, the results show that even increasing the ITO emissivity does not effectively suppress the substrate influence.*

Keywords: *infrared thermography, heat transfer, IR absorption, boiling.*

1. INTRODUCTION

Infrared thermography is a non-intrusive technique that allows measuring time-dependent surface temperatures with high temporal and spatial resolutions. If correctly calibrated, high accuracy is also achieved, if not, the measurements merely serve as a qualitative indication of the temperature of the object. Although many heat transfer processes can be well described by time-averaged and localized measurements, such as temperature measurements from thermocouples, they possess dynamic characteristics that can be better understood once accurate time-resolved measurements with high spatial resolution, such as those provided by infrared thermography, are available. For instance, Su et al. (2018) observed that under steady annular flows, the surface temperature oscillates coherently with the interfacial waves of the liquid film; Korniliou et al. (2018) observed that the heat transfer coefficient during slug flows in a rectangular microchannel presented a maximum at the channel centerline while during annular flows, dryout occurred preferentially at the channel edges.

To allow optical access to the surface under study in the IR spectrum, the test section must be carefully designed. Typically, two methods have been used for that: (i) a metal foil or electrically conductive channel covered with a high emissivity paint on the outside surface (Visentini et al. (2014), Teodori etal. (2018), Kingston et al. (2018)); (ii) a thin conducting film deposited on an IR transparent or semi-transparent substrate (Fischer et al. (2014), Bucci et al. (2016), Su et al. (2018)). The film heater is in direct contact with the fluid and the substrate is interposed between the heater and the camera. Configuration (i) has the advantage of being simple and allowing the use of a polynomial curve fit to map the IR signal into surface temperatures, however, the heat diffusion through the channel wall damps the temperature variations

of the inner wall, limiting the observed time scales. Additionally, the thin foil is not representative of real surfaces due to its low heat capacity (Bucci et al. (2016)). Configuration (ii) is more complex, considering both its manufacturing process and the data reduction procedures, however, it allows the evaluation of the inner surface temperature without thermal damping effects. Depending on the substrate optical properties, its contribution to the IR signal reaching the camera sensors can be compensated by calibration curves derived under uniform temperature conditions or the contribution of the substrate in the irradiation reaching the camera must be determined based on theoretical models. For instance, if the substrate used has negligible absorption, which is the case of calcium fluoride (CaF_2), then the calibration curve can be directly applied, because the influence of the substrate is negligible (Fischer et al. (2014)). However, CaF_2 is fragile and its use under conditions where intense boiling or high temperature gradients may be encountered is not recommend, because it easily breaks. On the other hand, sapphire presents better mechanical properties, but its IR absorption is non-negligible, which makes necessary data reduction techniques based on theoretical models, as proposed by Kim et al. (2012) and Bucci et al. (2016). Essentially, the idea behind these models is the same, separate the irradiation reaching the camera into heater, substrate, and ambient radiation. The main difference between them is that Kim model employs uniform optical properties, while Bucci model employs wavelength dependent optical properties. Both choices are justified based on the materials chosen by each author to manufacture the test section: Kim et al. (2012) used silicon, which has approximately uniform absorption coefficient in the wavelength range detected by the camera; Bucci et al. (2016) used sapphire, which has wavelength-dependent absorption in the wavelength range of interest.

In this work, both models are compared to the curve fit approach for an ITO-sapphire heater. Since the analysis carried out in this work is focused on the use of IR thermography to evaluate heat transfer during convective boiling of water under conditions close to wall dryout and during intense bubble nucleation, sapphire was chosen for the analysis. A sensitivity study of Bucci et al. (2016) model is also presented to evaluate the parameters that influence the most in the results.

2. DESCRIPTION OF THE MODELS

Kim et al. (2012) and Bucci et al. (2016) models are similar, with the only difference being the use of uniform optical properties by the first and wavelength dependent properties by the second. The equations of the Bucci model are given below, while Kim model equations can be found in Kim et al. (2012). Basically, the irradiation of each component of the test section is calculated based on its optical properties and temperature, as illustrated in Figures 1 and 2, to provide the total irradiation reaching the camera sensor:

$$E_{camera} = E_{ITO} + E_{amb} + E_{sapphire} \tag{1}$$

$$E_{ITO} = \int_{\lambda_1}^{\lambda_2} E_{p\lambda,T_{ITO}} \tau_{\lambda,app} d\lambda \tag{2}$$

$$E_{amb} = \int_{\lambda_1}^{\lambda_2} E_{p\lambda,T_a} \rho_{\lambda,app} d\lambda \tag{3}$$

$$E_{safira} = \int_{\lambda_1}^{\lambda_1} E^{s-}_{p\lambda,T(z)} \varepsilon^{-}_{\lambda,app} d\lambda + \int_{\lambda_1}^{\lambda_2} E^{s+}_{p\lambda,T(z)} \varepsilon^{+}_{\lambda,app} d\lambda \tag{4}$$

where $E_{p\lambda}$ is the spectral emissive power of a blackbody, defined as:

$$E_{p\lambda}(\lambda, T) = \frac{2\pi h_p c^2}{\lambda^5 [exp(h_p c / k\lambda T) - 1]} \tag{5}$$

and h_p and k are Planck and Boltzmann constants, and c is the speed of light in vacuum.

The apparent properties (*app*), appearing in Eqs. (1) to (4), account for multiple reflections at the ITO-sapphire (*IS*) and sapphire-air (*sa*) interfaces. The relations are given below, while their derivations can be found in Bucci et al. (2016).

$$\tau_{\lambda,app} = \frac{(1-\rho_{\lambda,IS})\tau_{\lambda,s}(1-\rho_{\lambda,sa})}{1-\rho_{\lambda,IS}\rho_{\lambda,sa}\tau^2_{\lambda,s}} \tag{6}$$

$$\rho_{\lambda,app} = \rho_{\lambda,app} + \frac{\rho_{\lambda,sa}\tau^2_{\lambda,s}(1-\rho_{\lambda,sa})^2}{1-\rho_{\lambda,IS}\rho_{\lambda,sa}\tau^2_{\lambda,s}} \tag{7}$$

$$\epsilon^{-}_{\lambda,app} = \frac{\rho_{\lambda,IS}\tau_{\lambda,s}(1-\rho_{\lambda,sa})}{1-\rho_{\lambda,IS}\rho_{\lambda,sa}\tau^2_{\lambda,s}} \tag{8}$$

$$\epsilon^{+}_{\lambda,app} = \frac{(1-\rho_{\lambda,sa})}{1-\rho_{\lambda,IS}\rho_{\lambda,sa}\tau^2_{\lambda,s}} \tag{9}$$

The apparent optical properties of the heater and the absorption coefficient of the sapphire used by Bucci et al. (2016) and Kim et al. (2012) models are shown in Figure 2. It can be seen that the apparent properties are influenced by the spectral dependency of the sapphire absorption coefficient, and this influences the results given by each model. Since both ITO and sapphire contributions depend on temperature, the transient heat conduction equation, Eq. (10), is solved in the substrate with imposed temperature on the ITO region (a portion of the upper surface) and natural convection on the other surfaces, as illustrated in Figure 1 for a 2D case. It was assumed that the first layer of the sapphire was at the same temperature of the ITO and that all heat transfer coefficients (HTC - h) were equal. Then the radiation model, Eqs. (1) to (9), is solved.

$$\frac{\partial T}{\partial t} = \alpha \nabla^2 T \tag{10}$$

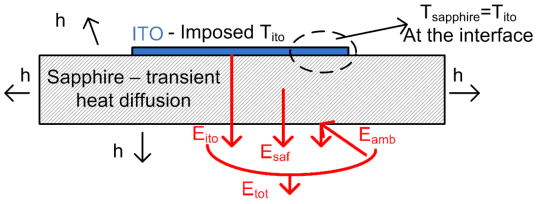

Figure 1 - Schematic of the model simulated to obtain the temperature field in the sapphire. Boundary conditions: HTC (h) at every surface except at the ITO region (in blue), where the temperature was imposed.

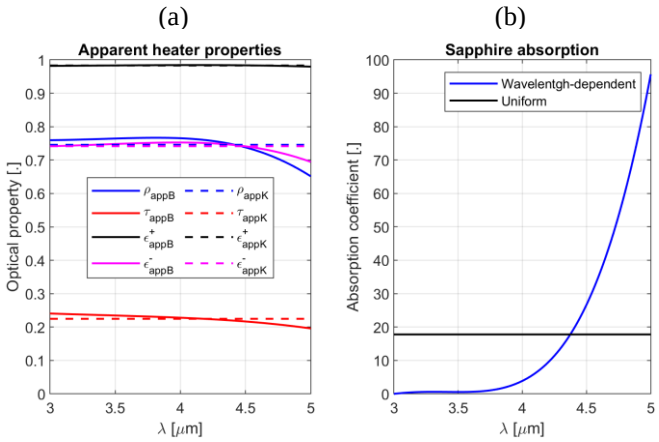

Figure 2 - Optical properties of the heater used by Kim et al. (2012) (K) and Bucci et al. (2016) (B) models. (a) Apparent properties, (b) sapphire absorption coefficients

3. NUMERICAL DATABASE

To perform the analysis, the database consisting of simulated IR images was generated numerically with the following approach:

a) Solve the transient heat diffusion in the sapphire substrate for various temperature functions imposed to the upper surface of the sapphire. It was considered that the temperature at this surface is the same as that of the ITO and that the other faces of the sapphire were exposed to air at 24°C and an HTC of 10W/m^{2}K (see Figure 1). A fourth order finite difference scheme was use for the spatial discretization while an explicit fourth order Runge-Kutta method was used for time marching.

b) Calculate the irradiation from the test section using Bucci et al. (2016) model and from that obtain the IR images and derive the calibration curve. Here it was considered that this model represents the physics of the problem more accurately than Kim et al. (2012) model, because it uses wavelength-dependent optical properties.

4. ANALYSIS - ONE DIMENSIONAL CASES

4.1 Solution procedures

Each model was applied with the solution algorithm proposed by each group of authors, with minor changes. The flowcharts in Figure 3 show both algorithms. The initial condition is unknown, so the approach was to estimate the ITO temperature based on the calibration curve and from that, calculate the steady-state solution of the sapphire temperature field and use that as the initial condition. The ambient contribution to the total radiation is a constant since ambient temperature is fixed. To solve for every time step, first an estimate of the ITO temperature in time t+dt is made using the calibration curve. Then the sapphire temperature distribution in t+dt is obtained by solving the heat diffusion PDE using the sapphire temperature distribution in time t and ITO temperature in times t and t+dt. Since the ITO temperature in t+dt is an estimate (assumed to be close to the actual value), the sapphire temperature in t+dt is also an estimate. Both

algorithms provide means to improve these estimates as the solution evolves. In Kim's method, the sapphire contribution to the radiation reaching the camera is calculated by solving the radiation model and obtaining the ITO contribution from Eq. (1). From that, a new estimate of the ITO temperature is obtained, considering the following equation:

$$E_{ITO} = F_{\lambda_1 \to \lambda_2} \bar{\varepsilon} \sigma T_{ITO}^4, \quad F_{\lambda_1 \to \lambda_2} = f(\lambda_1 T_{ITO}, \lambda_2 T_{ITO}) \tag{11}$$

where it is emphasized that the fraction of the total blackbody irradiation emitted in the spectral band ($F_{\lambda 1 \to \lambda 2}$) is not only a function of the spectral band, but also of the temperature of the body, so Eq. (11) is solved iteratively for the new estimate of T_{ITO}.

Although not initially proposed by Kim et al. (2012), the solution is iterated to assure convergence is reached (typically in 2 iterations). After that, it follows to the next time step.

In Bucci's method the first steps are the same as in Kim's method, but instead of applying Eq. (1) to obtain the ITO contribution, every contribution is obtained by solving the radiation model from the estimated temperatures. Then they are added to obtain an estimate of the total irradiation reaching the camera ($E_{estimated}$). The difference between measured and calculated irradiation is used to update the ITO temperature guess in an iterative process, such as:

$$T_{ITO}^{it+1} = T_{ITO}^{it} - \frac{E_{estimated} - E_{camera}}{\frac{dE_{cal}\left(T_{ITO}^{it}\right)}{dT}} \tag{12}$$

where *it* stands for the iteration and the denominator of the second term in the right-hand side (RHS) is the derivative of the calibration curve, evaluated at T_{ITO}.

The iteration stops when the second term on the RHS of Eq. (12) is lower than 10^{-4}. Then the algorithm moves to the next time step. In both methods, the heat diffusion PDE was solved using implicit schemes, to allow for large time steps while using a fine spatial grid and preventing instability of the solution.

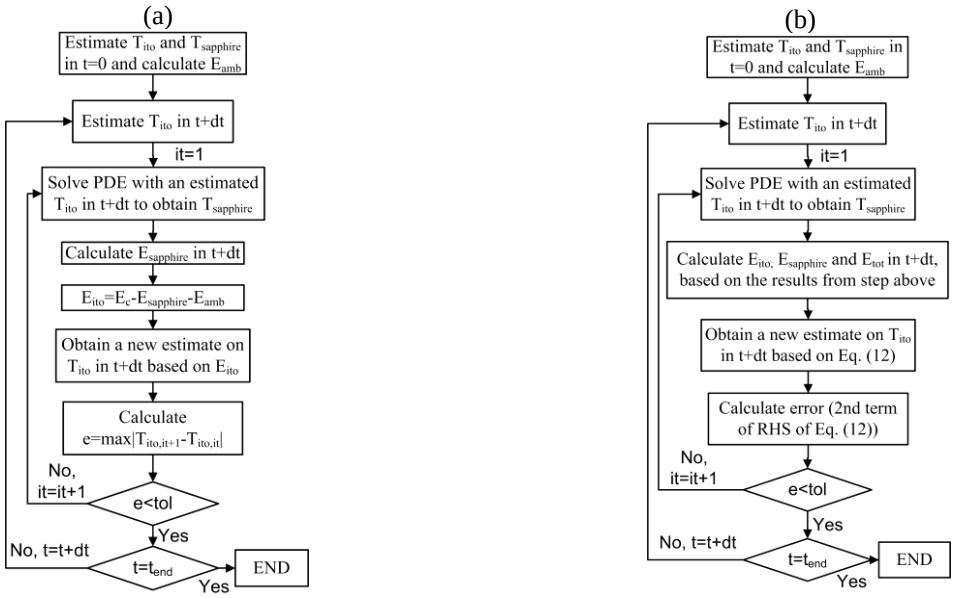

Figure 3 - Flowchart of Kim (a) and Bucci (b) models

Figure 4a presents a comparison between Kim et al. (2012) and Bucci et al. (2016) models considering uniform temperature in the substrate. The estimated radiative heat flux calculated by Bucci model was used to derive the calibration curve used in the following sections. Both models estimate non-negligible contributions from the sapphire and from the ambient to the total irradiation, but Kim model estimates a slightly larger contribution from the ITO and from the ambient and a lower contribution from the sapphire, as highlighted by the relative deviation shown in Figure 4b. From this figure, it can be expected that for a given experimental condition, Kim model will yield lower temperatures for the ITO. This comes from the fact that when solving the problem, the model matches the total irradiation measured by the camera with the estimated radiation from solving the model's equations. The curves derived under uniform temperatures show that for the same temperature, Kim model estimate larger emissions from the ITO, which means that to match the measured irradiation the model will estimate lower temperatures for this component.

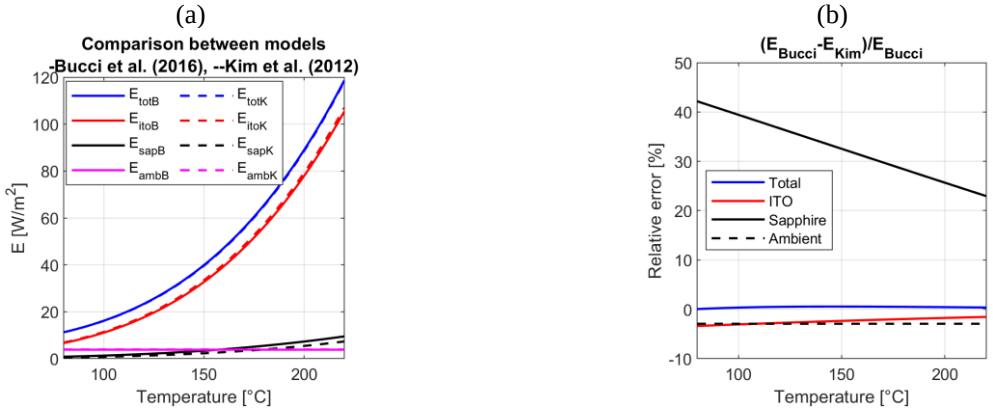

Figure 4 – Comparison between Kim and Bucci models: (a) predicted contributions considering uniform temperature on the test section, (b) relative deviation between models.

4.2 Sample cases

Figure 5 presents the results obtained using calibration curve, Kim and Bucci methods for an exponential increase of the ITO heating power, as performed by Bucci et al. (2016) to validate their model. The following analytical solution was obtained for the ITO temperature during the exponential heating. Here, this solution was used as the boundary condition of imposed temperature in Figure 1.

$$T_{ITO}(t) = T_0 + q^{"} e^{t/\tau} \Big/ \left[\frac{\varepsilon_s}{\sqrt{\tau}} tanh \frac{1}{\sqrt{\frac{\alpha_s \tau}{L_s}}} + \frac{\varepsilon_w}{\sqrt{\tau}} \right] \tag{13}$$

where T_0 is the initial condition, q" is equal to 6500W/m^2, ε are thermal effusivities of sapphire (s) and water (w), α_s is the thermal diffusivity of sapphire, L_s is the thickness of the sapphire and τ is the time constant of the power increase.

This figure highlights the effect of the substrate temperature non-uniformity on the results. Additionally, the effect of the sampling rate on Bucci model results is assessed by comparing five different sampling rates. Figures 5a-c show that Kim and calibration curve methods underestimate the ITO temperature. As anticipated in the beginning of this section Kim method errors are due to an overestimation of the ITO contribution, while the calibration curve method errors are due to the non-uniformity of the substrate temperature, shown in Figure 5d. Both methods yield errors that can be larger than 1.5°C, whilst Bucci method provides solutions with less than 0.5°C of error. It is also seen that decreasing the sampling rate increases the errors as time evolves. This is explained by the dissipative characteristic of implicit schemes used to solve the heat conduction in the substrate. Large time steps mean more dissipation in the results. Unfortunately, explicit schemes cannot be used due to their limited stability. Interestingly, in the interval from 0 to around 0.025s the lowest sampling frequency provided the best solutions. However, as time increases, so does the error, and higher sampling rates provide better solutions.

Figure 6 shows a comparison between the models for a sinusoidal excitation. The largest errors are encountered in the crest and in the trough of the wave. When the sampling rate is above 1kHz approximately, the use of Kim or Bucci methods is justifiable, because they provide better estimations to the exact temperature. However, if the sampling rate is decreased, there is not much improvement in using complex data reduction techniques, see for instance the solution using Bucci model with sampling rate of 250Hz and the calibration curve method. One common feature of all the solutions is that they estimate lower temperatures in the wave crest and larger temperatures in wave trough. In the case of the calibration curve, the non-uniformity of the sapphire temperature profile, shown in Figure 6e, explains why this happens: when the ITO temperature is at the crest of the sine wave, the rest of the substrate is at lower temperatures, due to heat diffusion. Since the calibration curve was derived for a uniform temperature, the resulting estimation is lower than the actual value. When the ITO temperature is at the trough of the wave, the substrate is at a higher temperature, which means that the estimation using the calibration curve will yield a higher value than the exact one. As for Kim method, the dissipation of implicit schemes used to solve the heat conduction and the overestimation of the ITO contribution to the total irradiation explains this behavior. For Bucci method, the dissipation of the implicit scheme is what caused the deviations in the solution.

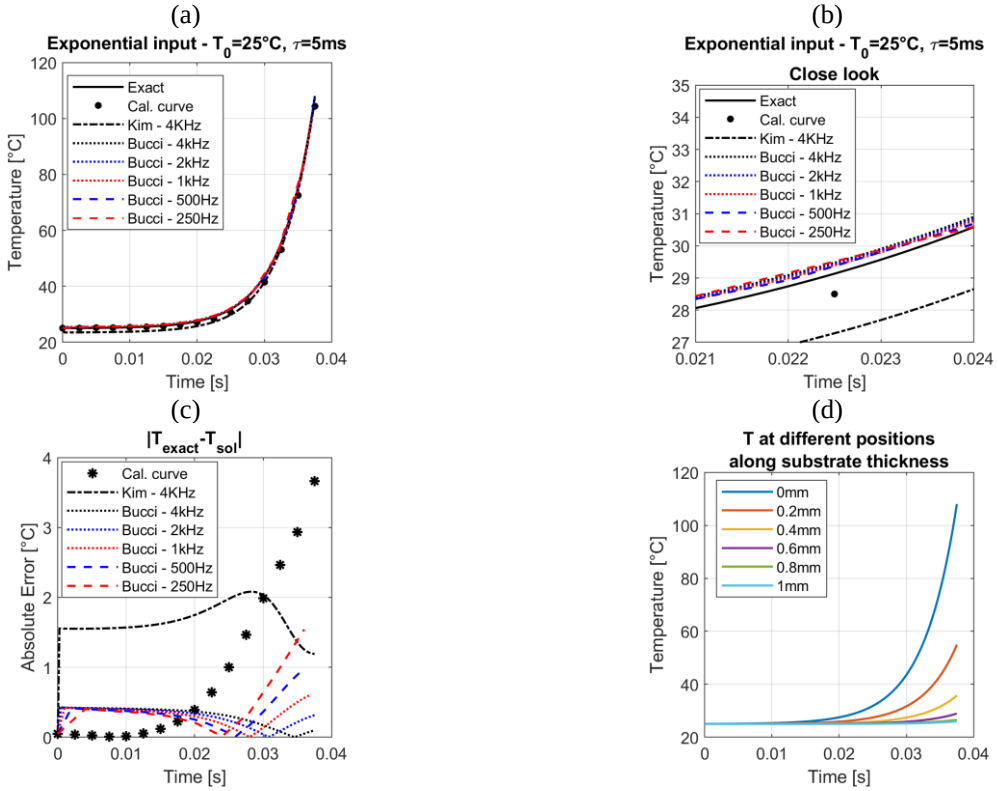

Figure 5 – Various results comparing the three methods for an exponential input, highlighting the effect of the sampling rate: (a) From 25 to 110°C; (b) Close look at the results; (c) Absolute error of each solution; (d) Temperature of the substrate along its thickness.

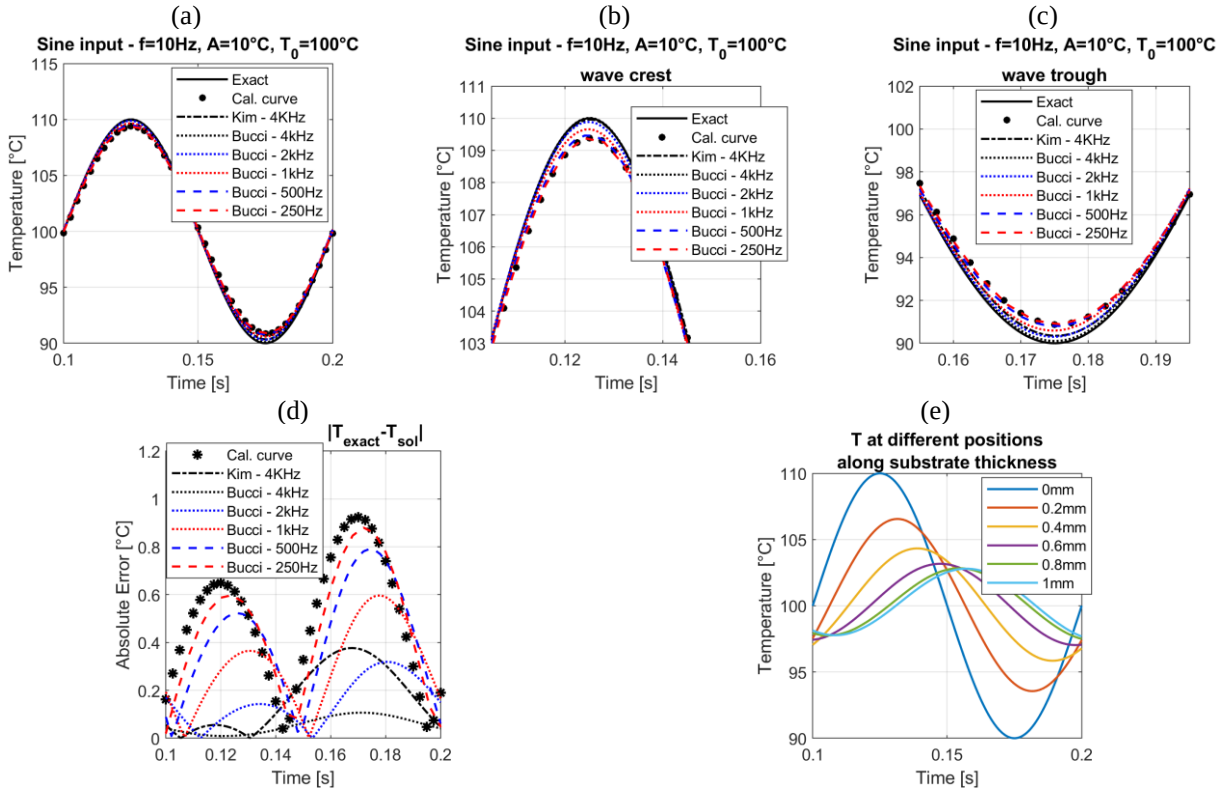

Figure 6- Various results comparing the three methods for a sinusoidal input, highlighting the effect of the sampling rate: (a) One period; (b) Close look at the wave crest; (c) Close look at the wave trough; (d) Absolute error of each solution; (e) Substrate temperature along its thickness.

4.3 Sensitivity analysis

The influence of each parameter of the model on the solution was assessed for Bucci model. During the database generation step the parameters were kept at the exact value, but during the solution step they were varied to evaluate their influence in the results. Figure 7a shows the results for the optical properties, Figure 7b, for the discretization along substrate thickness and, Figure 7c, for the heat transfer coefficient (h).

In the case of the optical properties, the influence of each property was assessed separately, that is, its value was decreased in 1% while keeping the others at the exact value. The properties varied were: sapphire absorption coefficient α_s, which is related to the sapphire transmissivity ($\tau_s=e^{-\alpha L}$); ITO-sapphire reflectivity ρ_{hs} which is related to the ITO emissivity ($\varepsilon=1-\rho$); sapphire-air reflectivity ρ_{sa}. From the uniform temperature curves shown in Figure 3a, it is expected that the ITO optical property is the most influential one, because the ITO contribution to the total irradiation measured by the camera is the largest. In Figure 7a, it can be seen that errors in sapphire absorption coefficient or the errors in the sapphire-air reflectivity do not compromise the solution, if the ITO-sapphire reflectivity is correctly known. In fact, in these cases the errors seem to be dominated by the errors in the solution procedure itself rather than the optical property knowledge, that is, the spatial discretization and time-marching errors. However, when the ITO-sapphire reflectivity is varied, the errors increase considerably. In the exponential case, at the end of the temperature excursion, the error surpasses 1°C while in the sinusoidal case it oscillates around 1°C.

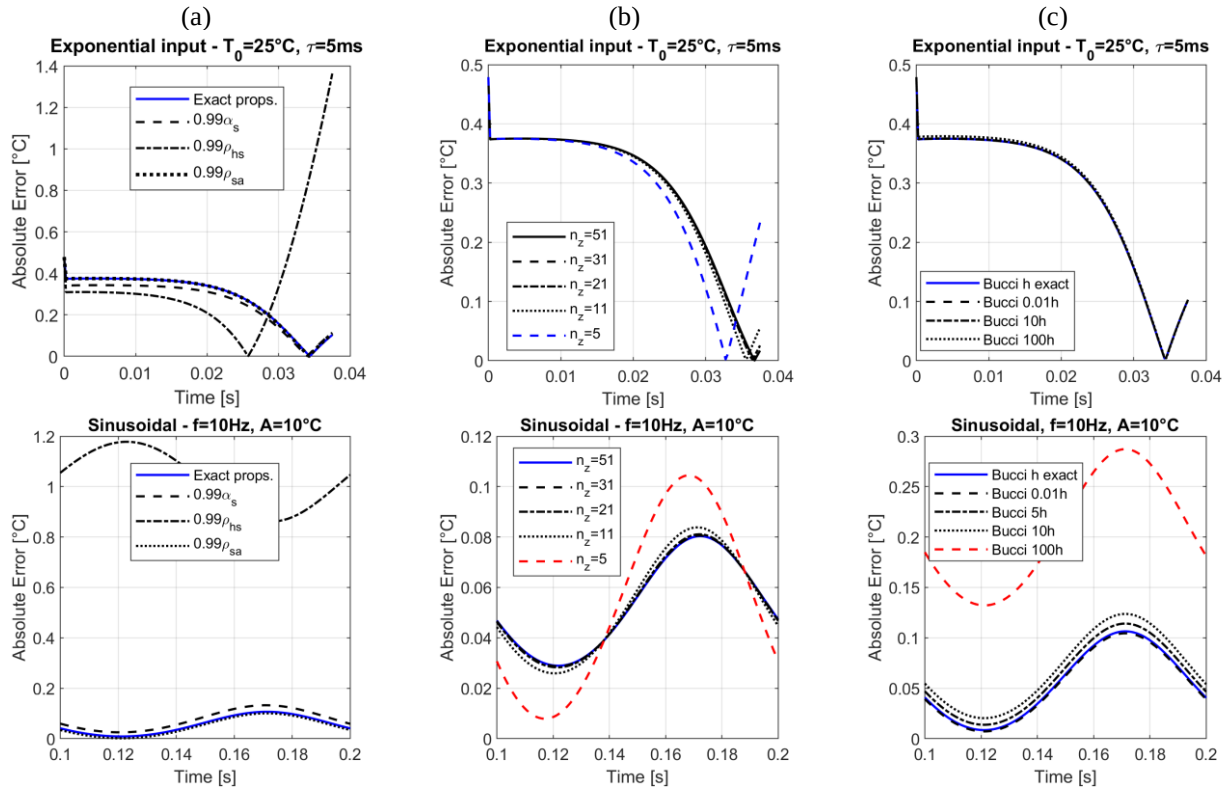

Figure 7 - Errors on the estimated temperatures. (a) optical properties variation. (b) spatial discretization. (c) heat transfer coefficient.

Figure 7b illustrates the effect of the spatial discretization in the solution. These figures show that a lower number of elements ($n \leq 5$) increases the error, because the accuracy of the solution of the heat diffusion equation decreases, consequently compromising the irradiation estimated by the model. However, as the number of elements is increased, there is a threshold where above it, additional improvements are not achieved. For the heater simulated in the present study, it seems that beyond 11 elements the added computational time to solve the problem is not worth the improvements in the solution.

Figure 7c shows the effect of the heat transfer coefficient (HTC) on the solution. For this, the HTC was varied from 0.1 to 1000 W/m^{2}K (0.01 to 100 times the exact value). These figures show that the HTC effect is minimal: to have a significant influence on the solution, the HTC had to be multiplied by 100 (HTC of 1000 W/m^{2}K), which is not realistic, since the outer surfaces of the heater are exposed to the ambient, exchanging heat by natural convection. This result corroborates by Bucci et al. (2016) statement, according to which the outer surfaces can safely be assumed adiabatic, because they do not affect considerably the result of the model.

Afterwards, a hypothetic case where the ITO-sapphire reflectivity was greatly reduced (thus increasing the emissivity) is analyzed. Jung et al. (2016) and Castanet et al. (2020) considered that, if the sapphire substrate was covered with a high emissivity paint, the calibration curve was sufficiently accurate for estimating the ITO temperature. Figure 8 shows that even with a high emissivity surface (two values were considered, 0.85 and 0.95) the sapphire contribution still affects the results if the substrate temperature is highly non-uniform. In the exponential case, shown in Figures 8a and 8b, from t=0 to t=0.15s, the substrate temperature is close to uniform, because the initial condition is 25°C and the surface temperature has not increased considerably yet. But as time increases and the temperature rises, the substrate temperature becomes non-uniform (refer to Figure 5b) and the error increases to above 1°C for ε=0.85 and 0.7°C for ε=0.95, when the calibration curve is used. However, when the sinusoidal case was simulated, Figure 8c, it was seen that if the sampling rate is below 500Hz, the errors obtained using the calibration curve are similar to the errors obtained applying Bucci model (~0.15°C), for both emissivities. Other cases where the calibration curve would result in accurate temperature measurements are when the substrate is thinner and a non-absorbing substrate is used, such as CaF_2, since the substrate effect would be reduced.

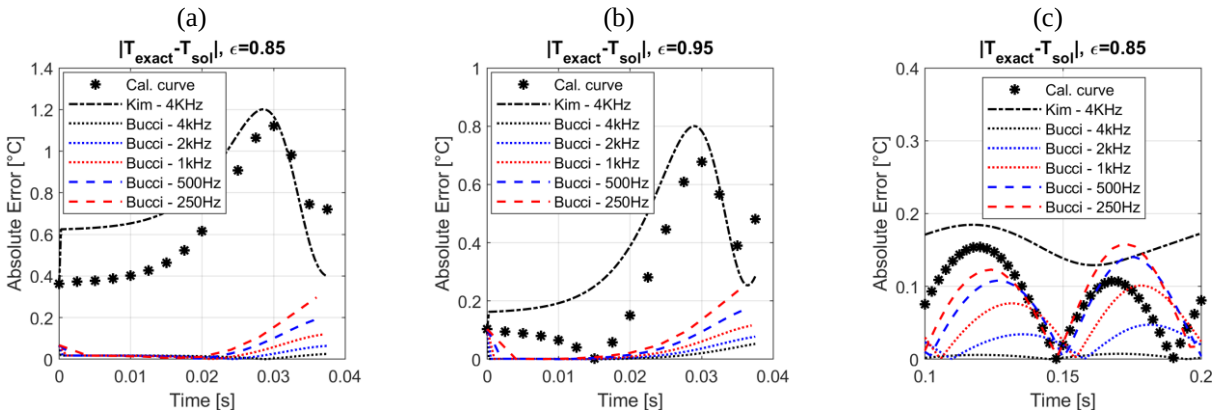

Figure 8 - Errors for the ITO temperature considering an ITO emissivity of 0.85 and 0.95. (a) Exponential case. (b) Sinusoidal case.

Furthermore, the thickness of the substrate influences directly on the solutions obtained by each model. As the thickness increases, the transmissivity of the substrate decreases and the signal reaching the IR camera sensor is progressively influenced by the substrate contribution. Table 1 presents mean absolute errors (MAE) and maximum absolute errors (MaxAE) of each data reduction technique for substrates thicknesses of 0.5, 1.0 and 1.5 mm. As the substrates thickens, MAE and MaxAE, due to application of a calibration curve or Kim model, increase because neither of these models are able to capture the substrate influence accurately. On the contrary, Bucci model errors stay almost constant since the model captures the influence of the substrate.

Table 1 – Mean and maximum errors for different substrate thicknesses

Type	Thickness [mm]	Calibration Curve		Kim		Bucci	
		MAE [°C]	MaxAE [°C]	MAE [°C]	MaxAE [°C]	MAE [°C]	MaxAE [°C]
Exponential	0.5	0.52	1.52	0.60	1.03	0.31	0.51
	1.0	0.88	3.66	1.67	2.08	0.31	0.43
	1.5	1.20	5.41	2.01	2.41	0.26	0.45
Sine	0.5	0.23	0.51	0.07	0.19	0.06	0.19
	1.0	0.50	0.99	0.17	0.40	0.06	0.11
	1.5	0.79	1.61	0.51	0.92	0.05	0.18

5. THREE DIMESIONAL CASE

As a last simulation, a three-dimensional case was run. A substrate of 25mm x 10mm x 1mm was simulated with four regions of temperature oscillations. To keep the database generation procedure simple, the oscillations were sinusoidal functions of time multiplied by gaussian functions of the space variables x and y, as follows.

$$T_{ITO}(x,y,t) = A\,sin(2\pi ft + \varphi)\,\frac{1}{\sigma\sqrt{2\pi}}exp\left(-\frac{1}{2}\left(\frac{(x-x_0)^2+(y-y_0)^2}{\sigma^2}\right)\right) \quad (13)$$

The frequency (f), amplitude (A) and phase (φ) were varied as well as the standard deviation of the gaussian (σ), meaning that each temperature oscillation would occupy different areas of the substrate. Figures 9a and 9b show two instants in time of the ITO temperature field in this simulation and Figures 9c and 9d show the errors resulted by regressing the data with Bucci model for the same instants in time. From top left to bottom right in each figure the frequency, amplitude and phase shift of each oscillation is: 15Hz, 25°C, 30°; 5Hz, 10°C, 0°; 10Hz, 10°C, 60°, and; 3.3Hz, 5°C, 30°. This figure shows the capability of the data reduction technique to recover the temperature field in a 3D case.

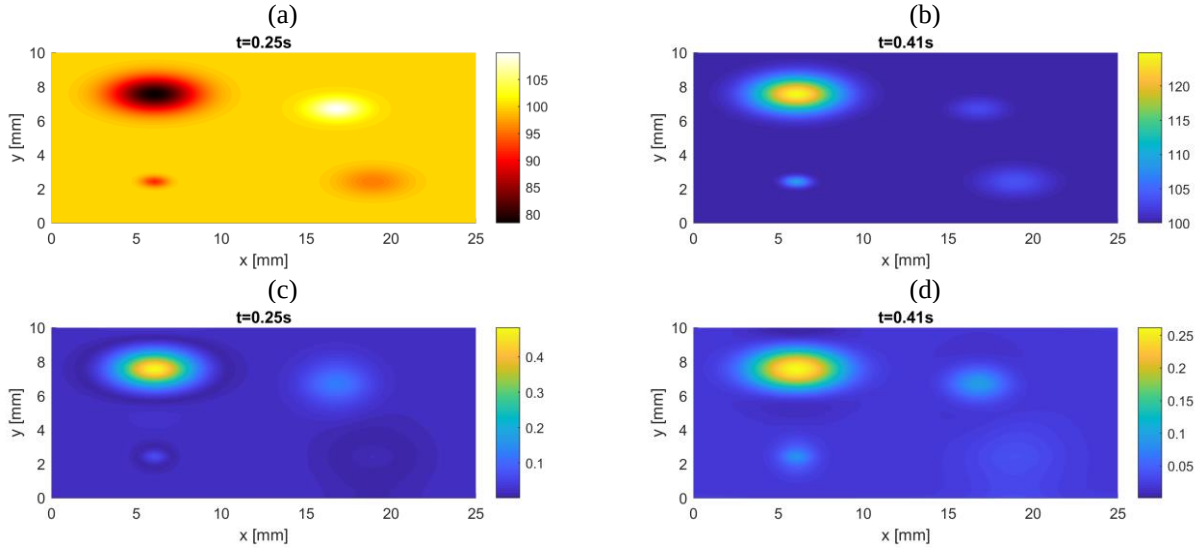

Figure 9 – Snapshots of the 3D case simulated. (a) and (b) Exact ITO temperature field (°C). (c) and (d) Absolute error of Bucci model (°C).

6. CONCLUSIONS

From the presented comparison between the data reduction/calibration techniques, it can be concluded that:

- The spectral dependency of the optical properties of the test section must be accurately known in order to apply complex data reduction models to calculate the heater temperature. In the case of an ITO-sapphire heater, the emissivity (which is low) is the most important parameter, because an error of only 1% in its value could cause the error in the estimated temperature to jump from around 0.2°C to larger than 1°C;
- If the emissivity of the ITO is increased, the errors fall accordingly, because the substrate contribution reduces. However, even in this case, the substrate influence is still present and Kim model and the calibration curve method present larger errors than Bucci model, when the substrate temperature field is highly non-uniform;
- The spatial discretization along the thickness of the substrate and the HTC considered during the solution procedure are less important parameters for the solution procedure than the optical properties. For the first, there is a threshold number of elements that produce an accurate solution and for the second, considerable influence was only seen when the HTC was increased to unrealistic values;
- Bucci model advantage over the other methods is more pronounced when the substrate temperature is highly non-uniform, which is expected in conditions close to the wall dryout in annular flows and conditions of intense bubble nucleation;
- The sampling rate is an important parameter for the correct estimation of the temperature. If too low, oscillations in the heater temperature might not be captured by the thermography and the solution procedure will be compromised. Additionally, the numerical solution of the heat diffusion equation, required during the data reduction procedure, has errors that increase as the time step increases.

7. ACKNOWLEDGMENTS

The authors gratefully acknowledge the financial support from FAPESP (São Paulo Research Foundation) through a Thematic grant under contract number 2016/09509-1 and Scholarship grants, 2019/01755-1 and 2020/10923-2. The second author also acknowledge the support of CNPq (National Counsel of Technological and Scientific Development of

Brazil) under Contract Numbers 305673/2017-3. This study was financed in part by the Coordenação de Aperfeiçoamento de Pessoal de Nível Superior - Brasil (CAPES) - Finance Code 001.

8. REFERENCES

Bucci, M., Richenderfer, A., Su, G.Y., McKrell, T., Buongiorno, J., 2016. A mechanistic IR calibration technique for boiling heat transfer investigations. Int. J. Multiph. Flow 83, 115–127. https://doi.org/10.1016/j.ijmultiphaseflow.2016.03.007

Castanet, G., Caballina, O., Chaze, W., Collignon, R., Lemoine, F., 2020. The Leidenfrost transition of water droplets impinging onto a superheated surface. Int. J. Heat Mass Transf. 160, 120126. https://doi.org/10.1016/j.ijheatmasstransfer.2020.120126

Fischer, S., Herbert, S., Slomski, E.M., Stephan, P., Oechsner, M., 2014. Local heat flux investigation during pool boiling single bubble cycles under reduced gravity. Heat Transf. Eng. 35, 482–491. https://doi.org/10.1080/01457632.2013.833048

Jung, J., Jeong, S., Kim, H., 2016. Investigation of single-droplet/wall collision heat transfer characteristics using infrared thermometry. Int. J. Heat Mass Transf. 92, 774–783. https://doi.org/10.1016/j.ijheatmasstransfer.2015.09.050

Kim, T.H., Kommer, E., Dessiatoun, S., Kim, J., 2012. Measurement of two-phase flow and heat transfer parameters using infrared thermometry. Int. J. Multiph. Flow 40, 56–67. https://doi.org/10.1016/j.ijmultiphaseflow.2011.11.012

Kingston, T.A., Weibel, J.A., Garimella, S. V., 2018. High-frequency thermal-fluidic characterization of dynamic microchannel flow boiling instabilities: Part 1 – Rapid-bubble-growth instability at the onset of boiling. Int. J. Multiph. Flow 106, 179–188. https://doi.org/10.1016/j.ijmultiphaseflow.2018.05.007

Korniliou, S., Mackenzie-Dover, C., Christy, J.R.E., Harmand, S., Walton, A.J., Sefiane, K., 2018. Two-dimensional heat transfer coefficients with simultaneous flow visualisations during two-phase flow boiling in a PDMS microchannel. Appl. Therm. Eng. 130, 624–636. https://doi.org/10.1016/j.applthermaleng.2017.11.003

Su, G.Y., D'Aleo, F.P., Phillips, B., Streich, R.M., Al-Safran, E., Buongiorno, J., Prasser, H.M., 2019. On the oscillatory nature of heat transfer in steady annular flow. Int. Commun. Heat Mass Transf. 108, 104328. https://doi.org/10.1016/j.icheatmasstransfer.2019.104328

Teodori, E., Pontes, P., Moita, A.S., Moreira, A.L.N., 2018. Thermographic analysis of interfacial heat transfer mechanisms on droplet/wall interactions with high temporal and spatial resolution. Exp. Therm. Fluid Sci. 96, 284–294. https://doi.org/10.1016/j.expthermflusci.2018.03.013

Visentini, R., Colin, C., Ruyer, P., 2014. Experimental investigation of heat transfer in transient boiling. Exp. Therm. Fluid Sci. 55, 95–105. https://doi.org/10.1016/j.expthermflusci.2014.02.026

9. RESPONSIBILITY NOTICE

The authors are the only responsible for the printed material included in this paper.